Supplementary Information

Simple Replica Micromolding of Biocompatible Styrenic Elastomers

Mark D. Borysiak, Kevin S. Bielawski, Nathan J. Sniadecki, Colin F. Jenkel, Bryan D. Vogt, and Jonathan D. Posner

Mechanical Properties

Mechanical properties of SEBS12 and SEBS42 are summarized in Table 1. The elastic modulus was calculated from the slope of stress-strain tensile curves with the standard deviation reported. The other properties listed in Table S1 are typical values reported by the manufacturer.[1]

Table S1. Summary of mechanical properties for SEBS12 and SEBS42

Polymer	Elastic modulus (MPa)	Elongation at break (%)	Tensile strength (MPa)	300% modulus (MPa)	Hardness (Shore A)
SEBS12	0.86 ± 0.12	600	10.34	N/A	35
SEBS42	6.18 ± 0.29	660	>34.47	6.45	65

Work of Adhesion Calculations

We calculate approximate interaction strengths between the polymer and substrate surface in an effort to predict the affinity of PS to preferentially segregate to the silicon, SU-8, and silane treated silicon surfaces. The interaction strength can be calculated by considering the work of adhesion, W_{12} that is required to separate two surfaces. This technique has successfully been used to predict the adsorption of different block polymers to cellulose substrates using molecular modeling to obtain energy values over a specified area.[2,3] We calculate work of adhesion for the various polymer-surface interactions using interfacial energy values.

The work of adhesion is the free energy change associated with the creation of two unit areas, 1 and 2 from contact between the two,

$$W_{12} = \gamma_1 + \gamma_2 - \gamma_{12} \quad . \tag{S1}$$

where γ_1 and γ_2 are the free energies of the two components and γ_{12} is the interfacial energy. The interfacial energy between two surfaces is the free energy change in expanding their interfacial area by unit area, predicted well by the harmonic mean equation for two solids,[5]

$$\gamma_{12} = \gamma_1 + \gamma_2 - \frac{4\gamma_1^d \gamma_2^d}{\gamma_1^d + \gamma_2^d} - \frac{4\gamma_1^p \gamma_2^p}{\gamma_1^p + \gamma_2^p} \quad \text{(S2)}$$

where the subscripts 1 and 2 refer to the two individual phases. The γ^d and γ^p correspond to the dispersion and polar components, accounting for the dispersion force interactions and the various dipolar/specific interactions respectively.[5] The overall surface energy is the sum of these two components,

$$\gamma_i^d + \gamma_i^p = \gamma_i \quad \text{(S3)}$$

where *i* denotes the media or surface.[5] The dispersion and polar components can be determined through contact angle goniometry measurements and are documented for many common polymers and surfaces.[5–7] Table S2 lists the dispersion and polar components, as well as the overall surface energy for each polymer and substrate.

Positive W_{12} values indicate attractive forces, with larger values corresponding to a larger amount of work being required to separate two surfaces, demonstrating greater attraction through dispersion and specific interactions. Work of adhesion values for the various polymer-substrate combinations are shown in Table S3. The net work of adhesion, ΔW_{12}, of the different blocks to the surface,

$$\Delta W_{12} = (W_{PS-surface} - W_{PEB-surface}) \quad \text{(S4)}$$

is calculated in order to see the differences between the polymer blocks affinity for each surface, where $W_{\text{PS-surface}}$ and $W_{\text{PEB-surface}}$ are the work of adhesion between the surface and the PS and

PEB blocks respectively.[3] When ΔW_{12} is large, there is a preferential interaction of one block component with the substrate.[8] The large PS ΔW_{12} for silicon and SU-8 in Table S3 indicate that PS should be more attracted to these surfaces than the highly hydrophobic silane surface.

The work of adhesion is also an important consideration when taking into account de-molding of the SEBS. Lower W_{12} values indicate less force required to de-mold the SEBS and thus help to preserve the integrity of the master molds. The low W_{12} values for silane in Table S3 make sense given that silane is often used as a mold release agent. Conversely, the high surface free energy of silicon wafers results in more difficult de-molding of SEBS, and thus greater likelihood of destruction of microstructures during de-molding The intermediate value of SU-8 allows for improved de-molding over silicon, but with more mold degradation than the silane treated surface.

Table S2: Summary of free energy values for the polymer blocks and substrate surfaces. The PE and PB values are average in the work of adhesion calculations.

(mJ/m^2)	PE[5]	PB[5]	PS[5]	Silane[7]	SU-8[6]	Silicon
γ_i^d	36.8	34.5	33.9	12.0	22.0	23.50
γ_i^p	0	0	6.8	0.40	4.5	36.80
γ_i	36.8	34.5	40.7	12.4	26.50	60.3

Table S3: Summary of work of adhesion for polymer/substrate interactions, net work of adhesion, and work of adhesion in medium 3, toluene. Large work of adhesion values indicate strong attraction between the polymer block and substrate. The net work of adhesion values indicate the relative strength of attraction between

Surface	Polymer	W_{12} (mJ/m^2)	ΔW_{12} (mJ/m^2)
SU-8	PS	64.2	9.7
	PEB	54.5	
Silane	PS	37.0	1.1
	PEB	35.9	
Si	PS	78.6	21.9
	PEB	56.7	
Phenethyl(silane)	PS	71.4	7.2
	PEB	64.2	

ToF-SIMS Analysis

Figure S1 shows the normalized positive ion spectra for SEBS42 (A), PS (B), and SEBS12 (C) cast on SU-8. SEBS42 (Figure S1A) contains both characteristic PEB (m/z = 41, 43, 55, 57, 69) and PS (m/z = 91, 103, 105, 115, 117) peaks, indicating that both polymers are present at the surface. The PS (Figure S1B) spectra consists of characteristic PS peaks, with a notable absence of large peaks in the C_3-C_5 clusters that result from PEB. The SEBS12 (Figure S1C) spectra lacks the significant characteristic PS peaks seen in Figure 1A and 1B, including the m/z = 91 peak that is the largest peak in the other two spectra. Peaks in the C3-C5 clusters that are largely characteristic of PEB dominate the SEBS42 spectrum.

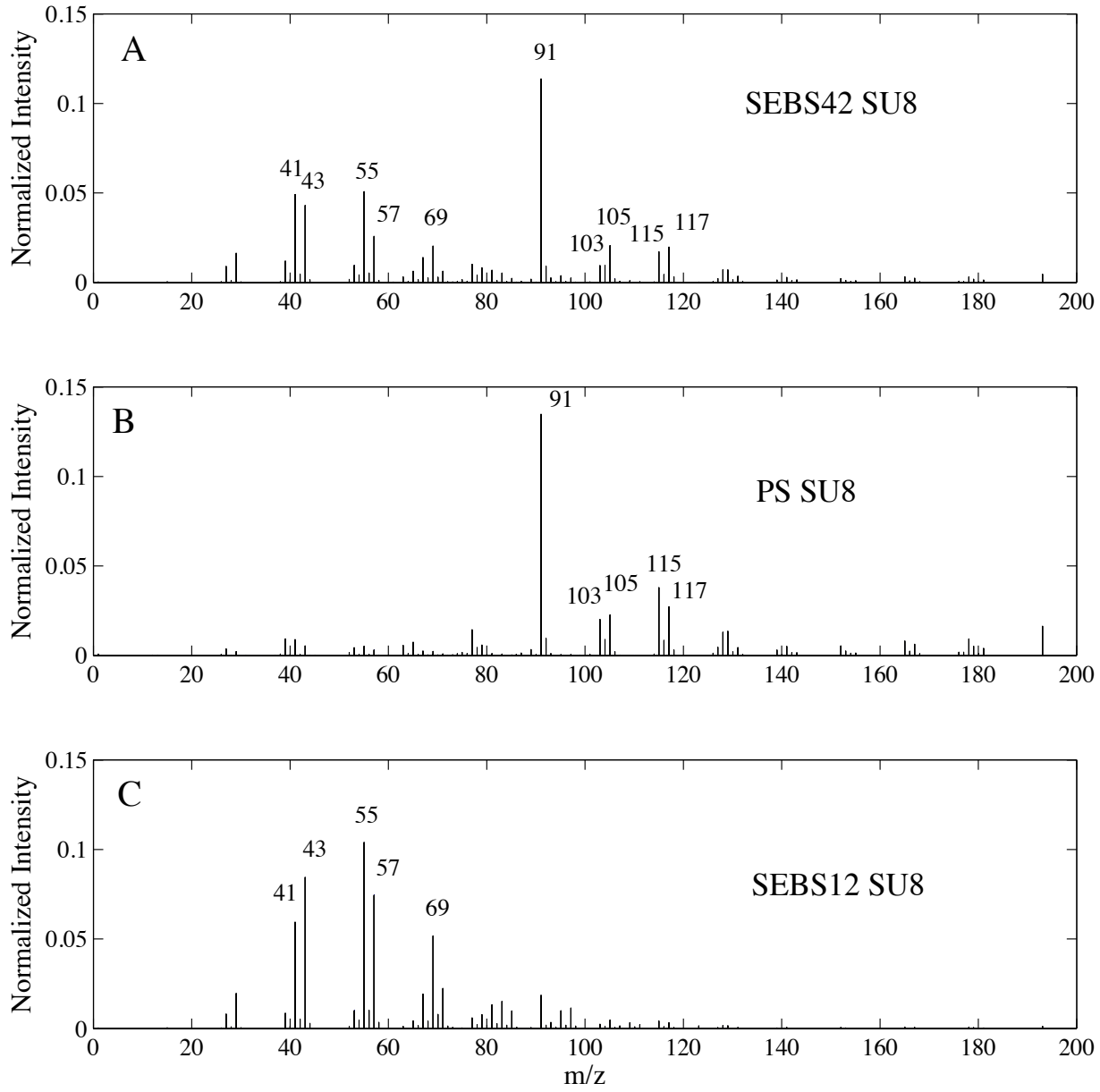

Figure S1. Normalized ToF-SIMS positive ion intensity profiles of SEBS42 (A), PS (B), and SEBS12 (C) cast on SU-8. The SEBS42 spectrum contains both characteristic PEB and PS peaks, while characteristic PEB peaks dominate the SEBS12 spectrum. Characteristic PEB peaks are absent in the PS spectrum. Major peaks for each spectrum are labeled.

Multivariate principal component analysis (PCA) was performed using the NESAC/BIO toolbox.[9] Graham and Castner have published a review of multivariate analysis for ToF-SIMS data from multicomponent systems.[10] We normalized the peak intensities of each spectrum by their total intensity in order to correct for differences in total secondary ion yield between the different spectrums. Root-mean centering set the mean of the data at the origin, ensuring that the variance in the data set was due to differences in the samples variances and not differences in the sample means. The principal components were calculated using the toolbox. We found that PC1 was responsible for 75% of the total variance in the system, which we attribute to the difference between the PS and PEB blocks at the surface of each sample. The first three principal components accounted for greater than 99% of the total variance, although PC2 and PC3 did not provide any meaningful information about the surface composition.

Loadings and scores plots for PC1 are shown in Figure S2A and Figure S2B. The loadings and scores give a concise summary of the original data and are interpreted together in order to see semi-quantitative trends between the samples.[10] The loadings give the relationship between the old variables (i.e., SIMS peaks) and the new variables (i.e., PC1) and shows which peaks are responsible for the separation of the samples in scores plot. The scores give the relationship between the samples in the new axis system. In general, samples with positive scores will have relatively higher peak intensities for the peaks with positive loadings, with the reverse true for negative scores and negative loadings.

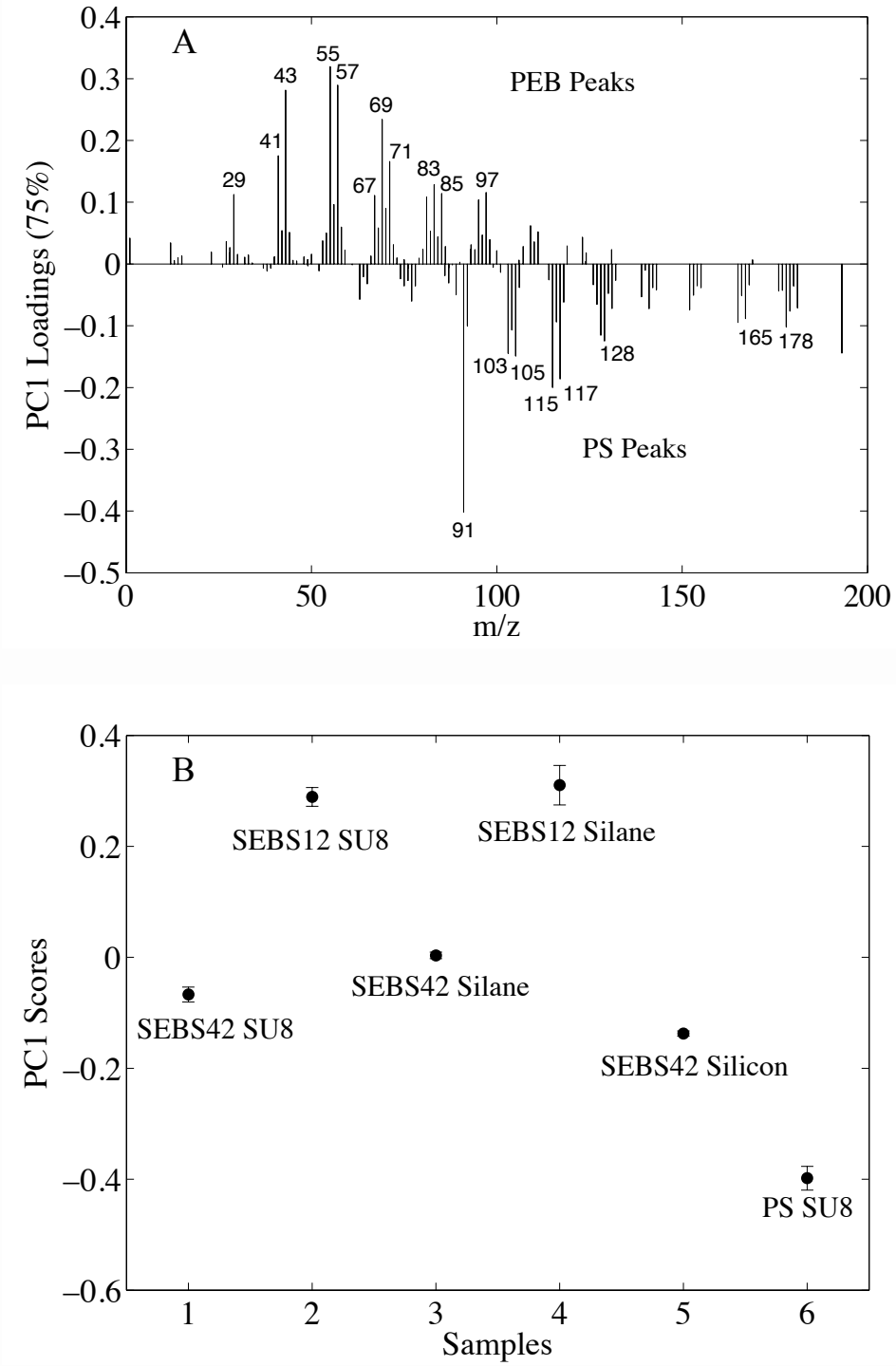

Figure S2. Principal component 1 (PC1) loadings (A) and scores (B). Positive loadings consist of characteristic PEB peaks and negative loadings consist of characteristic PS peaks. Thus, samples with positive scores have more PEB at the surface, while samples with more negative scores have more PS at the surface. SEBS42 has more negative scores than SEBS12 on similar casting surfaces, indicating greater PS composition. Samples have increasingly more PS when cast on silane, SU-8, and silicon respectively. Pure PS cast on SU-8 is shown as a reference. Error bars indicate 95% confidence intervals.

From Figure S2A, it can be inferred that the positive loadings correspond to the PEB block of the SEBS copolymer being at the surface, while the negative loadings correspond to the PS block of the SEBS copolymer being at the surface. The positive loading peaks in Figure S2A are predominantly characteristic peaks for ethylene[e] or both ethylene and butylene[eb] (m/z = 29[eb], 41[eb], 43[eb], 55[eb], 57[eb], 67[e], 69[eb], 71[e], 83[eb], 85[e], 97[eb]). The largest positive loading peaks (m/z = 41, 43, 55, 57, 69) are characteristic peaks that are shared by both ethylene and butylene, indicating these peaks are likely representative of the whole rubber segment of the block copolymer. Characteristic PS peaks dominate the negative loading peaks, with the most significant occurring at m/z = 91, 103, 105, 115, and 117. Since positive loadings correspond to positive scores and negative loadings correspond to negative scores, we can determine semi-quantitatively a comparative amount of PS at the surface for the tested samples. Positive scores will be indicative of higher PEB content at the surface compared to the other samples, while negative scores will indicate higher PS content at the surface compared to the other samples. The scores from Figure S2B are multiplied by 100 for clarity and reported in Table 2 in the full text.

The molar fraction of PS at the surface is defined by,

$$R = \frac{I_{PS}}{I_{PS} + I_{PEB}} \qquad \text{(S5)}$$

where I_{PS} and I_{PEB} are the total intensities of the characteristic ions from PS and PEB respectively.[11] In order for equation S5 to be valid, the characteristic ions used in the calculation must be absent of matrix effects.[11,12] A linear plot of bulk PS mole fraction versus calculated PS mole fraction for a random copolymer sample indicates an absence of matrix effects for the selected peaks. However, plots using block copolymers may not be perfectly linear, even in the absence of matrix effects, due to preferential attraction of one of the blocks to the surface. As a result, we choose an R^2 = 0.95 value as our arbitrary cutoff for peak selection to use for

calculating the molar fraction of PS at the surface. Combinations of the peaks with the five largest loadings for PS (m/z = 91, 103, 105, 115, and 117) and PEB (m/z = 41, 43, 55, 57, 69) from Figure S2A were plotted to examine the matrix effects of each peak. Each plot consists of a bulk PS mole fraction versus a calculated mole fraction (equation S5) for SEBS12, SEBS42, SEBS with 67 wt% PS, and PS cast on SU-8. Figure S3 shows an example plot for peaks m/z = 103 (I_{PS}) and m/z = 43 (I_{PEB}). Table S4 gives the R^2 values for the various peak combinations.

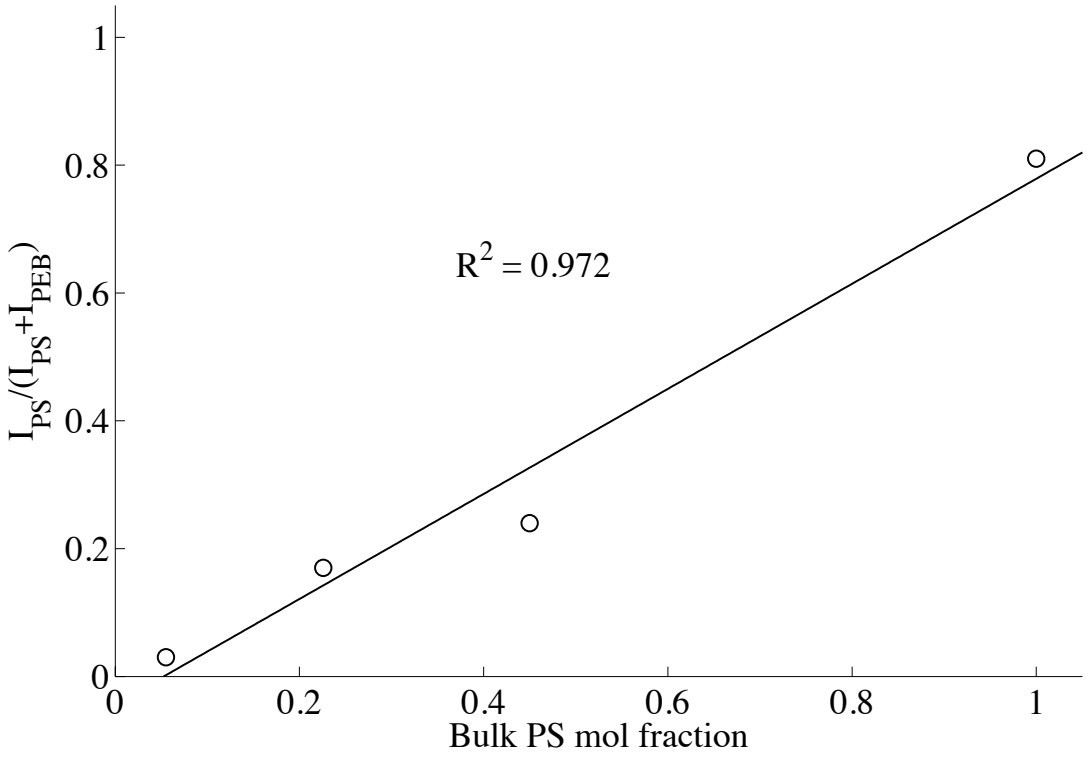

Figure S3. Plot of the bulk PS mole fraction versus the calculated PS mole fraction based off of the m/z = 103 (I_{PS}) and m/z = 43 (I_{PEB}) peaks for SEBS12, SEBS42, SEBS with 67 wt% PS, and PS cast on SU-8. The near constant slope (R^2=0.972) indicates that matrix effects are likely minimized or absent for these peaks.

Table S4. R^2 values for plots of bulk PS mole fraction versus calculated PS mole fraction, $I_{PS}/(I_{PS}+I_{PEB})$, for various peak combinations. The first row contains the PS peaks and the first column contains the PEB peaks. Each plot consists of SEBS12, SEBS42, SEBS with 67 wt% PS, and pure PS. The peaks used for calculation of the molar surface fraction of PS are bolded.

Peaks	91^{PS}	103^{PS}	105^{PS}	115^{PS}	117^{PS}
41^{PEB}	0.715	0.949	0.954	0.821	0.805
43^{PEB}	0.665	**0.972**	0.943	**0.981**	0.943
55^{PEB}	0.665	**0.962**	0.945	**0.987**	0.941
57^{PEB}	0.680	**0.982**	0.916	**0.953**	0.922
69^{PEB}	0.657	0.831	0.875	0.806	0.89

We chose the m/z = 103 and 115 peaks (PS) and m/z = 43, 55, and 57 (PEB) to calculate the molar surface concentration of PS for the various samples. These peak combinations have R^2 values greater than 0.95. Additionally, the m/z = 103 and 115 peaks have been noted as suitable characteristic peaks for quantifying a similar poly(styrene-butadiene) copolymer system, as well as other systems involving PS copolymers.[11–13] Other studies have noted that the m/z = 91 and 105 peaks exhibit matrix effects in certain systems and were not used in our calculation.[13,11] The low R^2 values for the m/z = 41 peak and to a lesser extent, the m/z = 69 peak indicate that these likely experience matrix effects as well. We also calculated the molar surface fractions of PS for a pure PS sample for various peaks, shown in Table S5.

Table S5. Molar surface fraction of PS for the pure PS samples, calculated using equation S5, $I_{PS}/(I_{PS}+I_{PEB})$, for selected peaks. Selected peaks are bolded.

Peaks	91^{PS}	103^{PS}	105^{PS}	115^{PS}	117^{PS}
41^{PEB}	0.94	0.70	0.73	0.82	0.77
43^{PEB}	0.97	**0.81**	0.83	**0.89**	0.84
55^{PEB}	0.96	**0.81**	0.83	**0.88**	0.85
57^{PEB}	0.99	**0.88**	0.89	**0.92**	0.91
69^{PEB}	0.99	0.91	0.92	0.95	0.95

Since the molar surface fraction for pure PS samples should be equal to 1, the selected peaks may be conservative estimates of PS surface fraction, as indicated by an average value of 0.86 for these peaks. The suggested matrix effects likely result in an overestimation of PS content for m/z = 91 and 69 and an underestimation of PS content for m/z = 41.

Table S6 shows the calculated surface PS molar concentrations (mol % PS) of the six chosen peaks, m/z = 103 and 115 for PS and m/z = 43, 55, and 57 for PEB, for the studied polymer/substrate combinations. The large deviations between the surface concentrations for the chosen peaks indicate the uncertainty in the calculations, but the semi-quantitative trends agree well with the PCA results, which utilize the entire spectrum.

Table S6. Surface molar concentration (mol% PS) of SEBS12 and SEBS42 cast on various substrates calculated using equation S5, i.e., $I_{PS}/(I_{PS}+I_{PEB})*100$. The average and standard deviations for each polymer/surface combination are reported in the full text.

Surface	Polymer		I_{PS} peaks	
		I_{PEB} peaks	*103*	*115*
SU-8	SEBS42	*43*	17.5	28.4
		55	15.3	25.3
		57	26.4	40.2
	SEBS12	*43*	2.67	4.78
		55	2.30	4.12
		57	3.08	5.50
Silane	SEBS42	*43*	9.5	17.4
		55	8.4	15.5
		57	16.4	28.1
	SEBS12	*43*	1.71	3.03
		55	1.43	2.55
		57	1.99	3.53
Silicon	SEBS42	*43*	26.4	40.6
		55	24.8	38.6
		57	36.7	5.25

Zeta Potential

We determined the zeta potential of SEBS42 by monitoring the electroosmotic flow of an electrolyte solution flowing through a microchannel fabricated in SEBS42. By determining the average velocity of the flow, the zeta potential can be calculated using the Smoluchowski equation. The Smoluchowski equation relates the mobility of particles, υ_E, and the zeta potential, ζ, during electrophoresis measurements,[14]

$$\upsilon_E = 4\pi\varepsilon_0\varepsilon_r \frac{\zeta}{6\pi\mu}(1+\kappa r) \tag{S6}$$

where ε_0 and ε_r are the relative dielectric constants and electrical permittivity of a vacuum respectively, μ is the solution viscosity, r is the particle radius, and κ is the Debye-Hückel parameter. For steady, one dimensional, and fully developed electroosmotic flow through a microchannel, the average velocity is given by

$$\upsilon_{av} = \frac{\varepsilon_r\varepsilon_0\zeta}{\mu}E_z \tag{S7}$$

where E_z is the applied electric field strength. The displacement of a lower concentration electrolyte solution by a higher concentration electrolyte solution in a channel can be monitored over a certain period of time to give the average velocity,

$$\upsilon_{av} = \frac{L}{\Delta t} \tag{S8}$$

where L is the total length of the channel. When two electrolyte solutions have a small concentration difference, the linear slope of the current-time relationship estimates the average electoosmotic velocity,

$$slope = \frac{\Delta I}{\Delta t} \tag{S9}$$

where ΔI and Δt are the changes in current and time over the linear range.

It can be shown that the zeta potential is then given by,[15]

$$\zeta = \frac{\mu \cdot slope \cdot L}{\varepsilon_r \varepsilon_0 E_z^2 A_{cross} (\lambda_{b1} - \lambda_{b2})} \quad \text{(S10)}$$

where A_{cross} is the cross sectional area of the channel and λ_{b1} and λ_{b2} are the bulk conductivities of the low and high concentration solutions. Table S7 gives typical values of the parameters for the zeta calculation. An example of a current-time plot is shown in Figure S4 for 9.5 and 10 mM phosphate buffer solutions, with an applied electric field of 200 V. The reported zeta potential is normalized by the negative logarithm of concentration,[16]

$$pC = -\log(c) \quad \text{(S11)}$$

where c is the molar concentration. The pC value for our experiment is 1.824, where c is the average of the 9.5 and 10 mM counterion concentrations (14.625 mM).

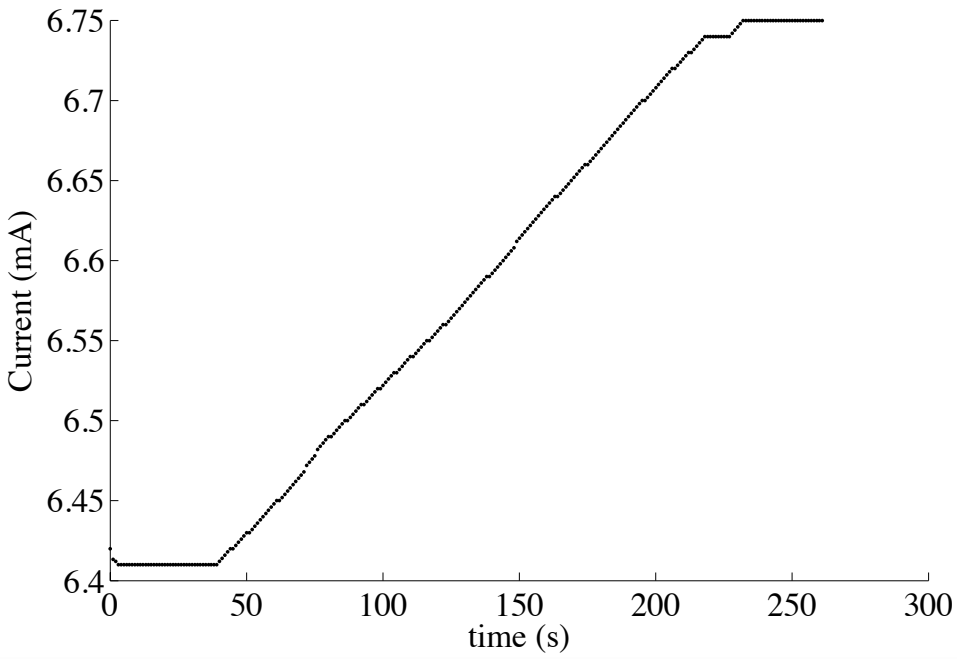

Figure S4. Current monitoring plot for 9.5 and 10 mM phosphate buffer solution electroosmotic flow in a microchannel. The slope from the linear region of the plot and equation S10 calculate the zeta potential for SEBS42.

Table S7. Typical values used with equation S10 for calculation of the zeta potential.

μ (Nsm^{-1})	L (m)	ε_0 (CVm^{-1})	ε_r	E_z (V/m)	A_{cross} (m^2)	λ_{b1} (S/m)	λ_{b2} (S/m)
0.001	0.040	8.85E-12	80	2.85E4	1.0E-8	0.1350	0.1290

Dye Adsorption and Absorption

Figure S5 shows the adsorption and absorption of 100 μM rhodamine B dye following incubation at room temperature for 24 h. The results of the long-term incubation are essentially identical to the short-term incubation shown in the main text.

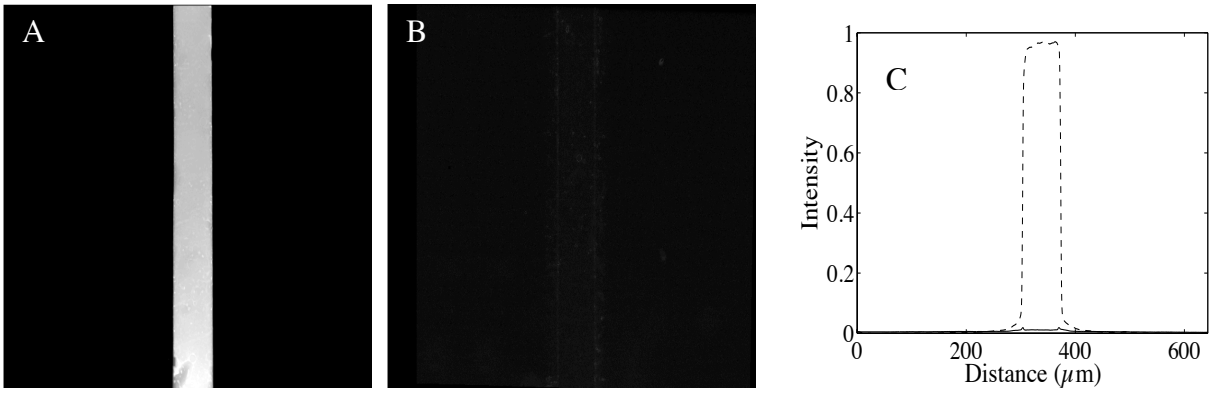

Figure S5. Images of (A) 50 μm wide SEBS42 channel filled with 100 μM rhodamine B solution for 24 h and (B) following rinsing with DI water. Normalized spectra of average intensity in the y-direction (C) show that there is little to no absorption of the dye in the channel (dashed line), even after the increased incubation period. Additionally, the adsorption of the dye following rinsing (solid line) is minimal.

Cell Culture

Figure S6 shows the cell growth for the 3T3 and BPAEC cells after six days of culture. Consistency in the cell shape is observed for all the surfaces. Additionally, surfaces that are not statistically different in Figure 3 show similar degrees of confluence for both cell types.

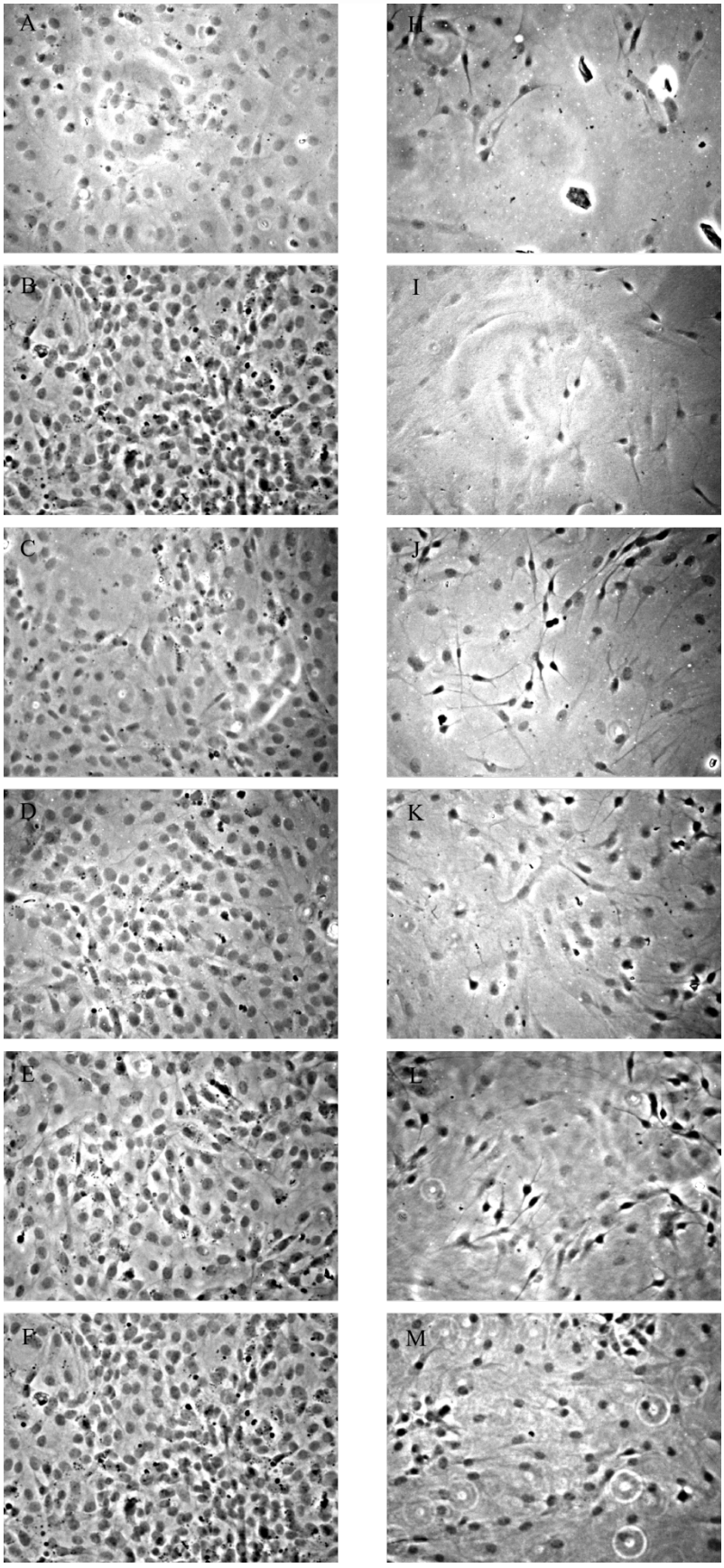

Figure S6. Cell morphology and growth. 3T3 cells appear similar in shape and degree of confluence after six days in culture on a variety of materials: (A) native SEBS, (B) ozone treated SEBS, (C) FN treated SEBS, (D) FN and ozone treated SEBS, (E) FN treated PDMS, and (F) TC dish. BPAEC cells have similar shape and degree of confluence after six days in culture on a variety of substrates (H) native SEBS, (I) ozone treated SEBS, (J) FN treated SEBS, (K) FN and ozone treated SEBS, (L) FN treated PDMS, and (M) TC dish.

Autofluorescence

Normalized autofluorescence spectra of SEBS42 and standard PS cuvettes are shown in Figures S7 and S8 respectively. The excitation scans range from 200-800 nm in 10 nm intervals with emission scans from 200-800 nm for each excitation. The SEBS42 has low autofluorescence through essentially the entire measured spectrum. It experiences a small amount of fluorescence from 300-600 nm, similar to PS, as seen in Figure S7 and S8. The fluorescence intensity in this region is higher than PS, but still relatively low. The two spectra are normalized by the overall maximum and minimum intensity between the two scans to compare the relative amounts of fluorescence between the two samples.

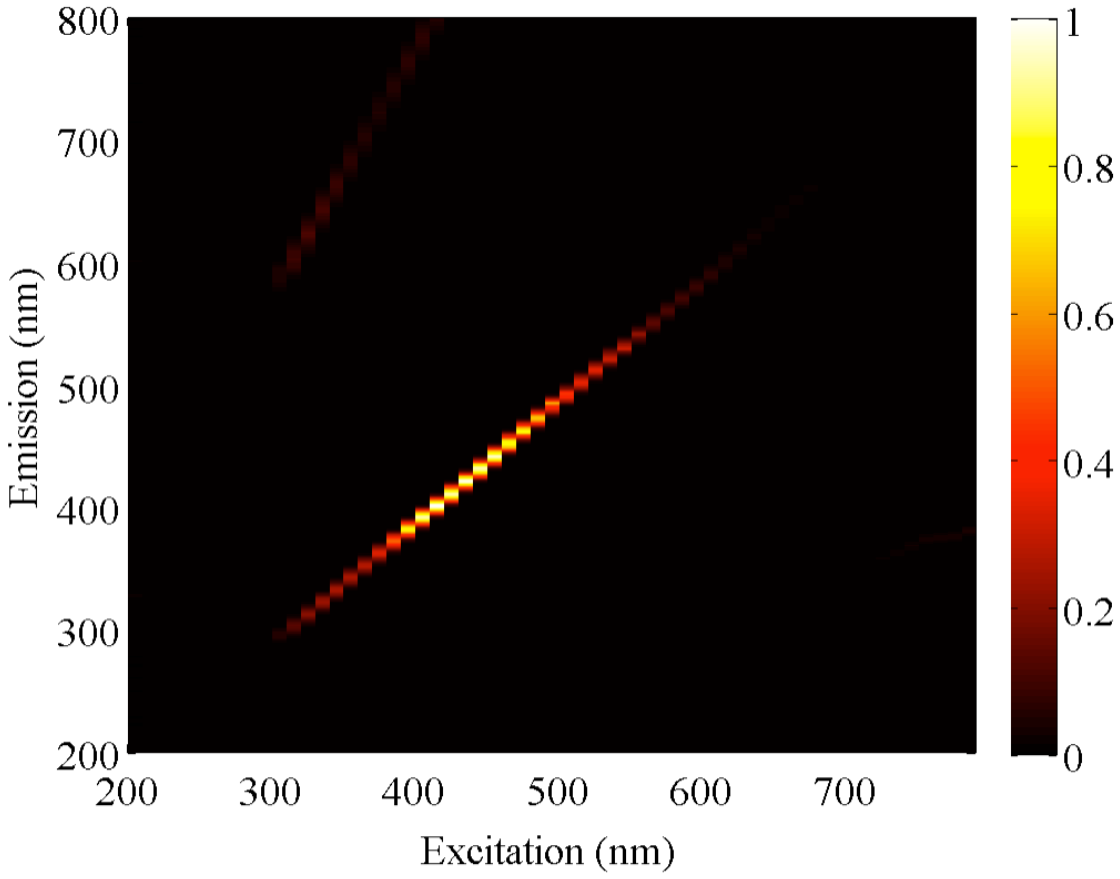

Figure S7. Autofluorescence spectra of SEBS42 ranging from 200-800 nm. The intensity is normalized by the overall maximum and minimum intensity between the SEBS42 and PS

(Figure S8) spectra for comparative purposes. SEBS42 overall has very low autofluorescence, with a narrow band of fluorescence between 300-600 nm. This also occurs, albeit to a lesser degree, in the PS cuvette standard.

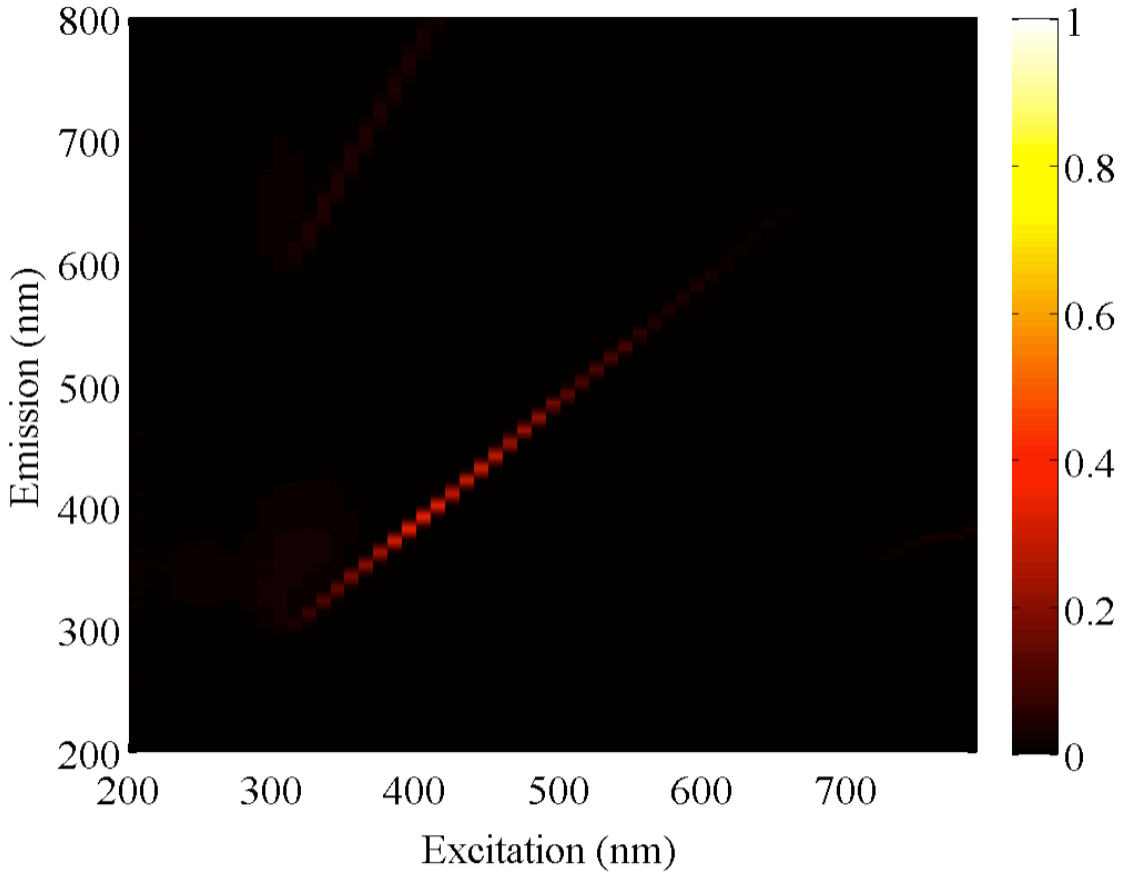

Figure S8. Autofluorescence spectra of PS ranging from 200-800 nm. The intensity is normalized by the overall maximum and minimum intensities between the SEBS42 (Figure S7) and PS spectra for comparative purposes. PS overall has very low autofluorescence, with a narrow band of excitation and emission between 300-600 nm.

Differential Scanning Calorimetry

DSC measurements were made on three SEBS42 samples to determine its thermal stability over temperatures relevant to microfluidic operation. The samples were heated at a rate of 5°C/min, with Figure S9 showing a typical result. The glass transition occurs around 75-85°C,

but is very mild, as noted by the lack of a significant peak or step in the curve, demonstrating the relative thermal stability of SEBS42.

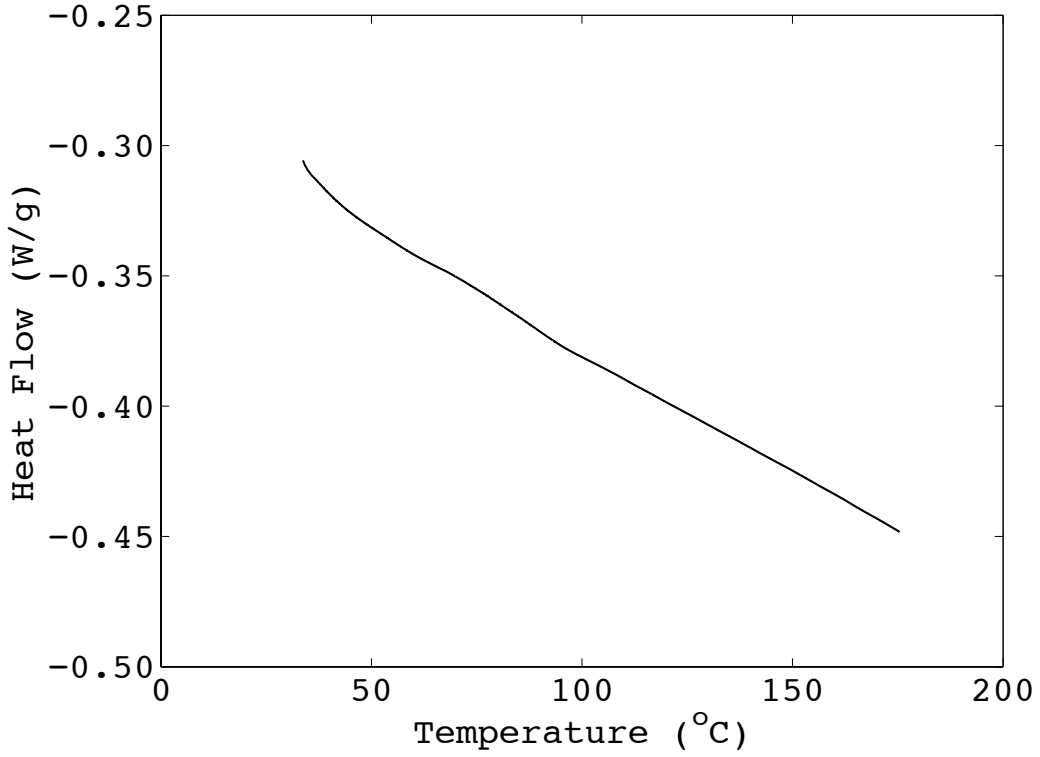

Figure S9. DSC measurement of SEBS42 with a temperature increase of 5°C/min. A slight step in the curve is seen around 75-80°C, corresponding to the glass transition of the material. However, this transition is very mild and does not significantly affect the practical use of the device around these temperatures.

Receding Contact Angle Measurements

Figure S10 shows the receding contact angle measurements following oxygen plasma treatment for SEBS42 and SEBS12. The receding contact angle measurements follow similar trends to the advancing contact angles.

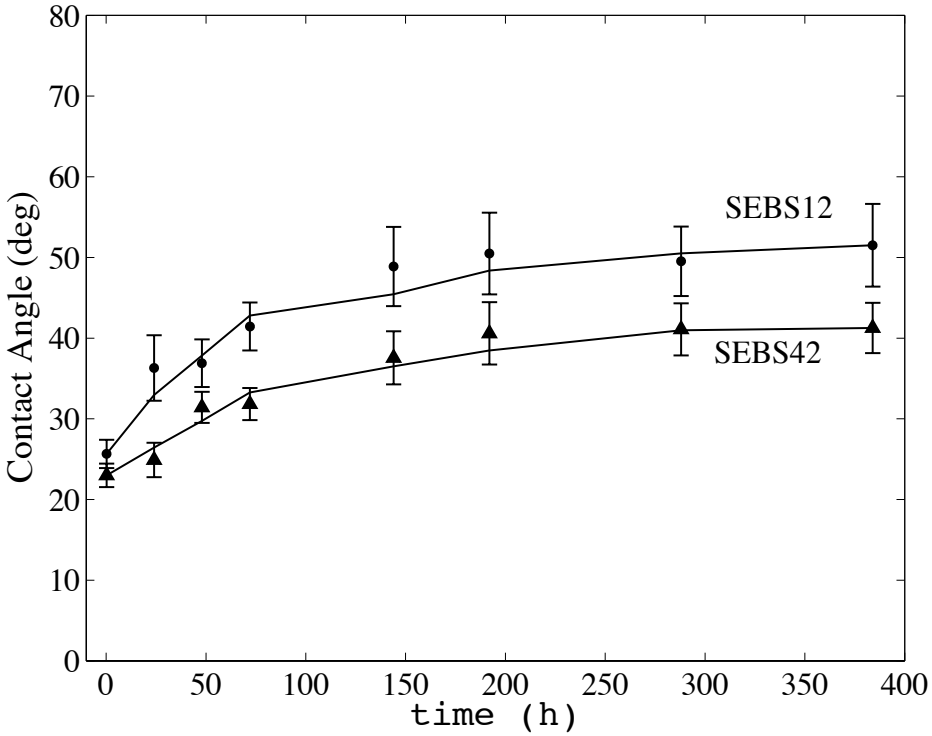

Figure S10. Receding contact angle measurements of oxidized SEBS12 (close circles) and SEB42 (closed triangles) surfaces cast on SU-8. The surfaces undergo hydrophobic recovery similar to the advancing angles. The SEBS12 is more hydrophobic due to less PS at the surface and in the bulk.

References

1. Kraton Polymer, *SEBS A1536H Copolymer Material Data Sheet*.
2. G. Chauve, L. Heux, R. Arouini, and K. Mazeau, *Biomacromolecules*, 2005, **6**, 2025–2031.
3. Y. Li, H. Liu, J. Song, O. J. Rojas, and J. P. Hinestroza, *ACS Applied Materials & Interfaces*, 2011, **3**, 2349–2357.
4. J. N. Israelachvili, *Intermolecular and Surface Forces*, Elsevier Inc., 3rd edn., 2011.
5. J. Brandrup, E. H. Immergut, E. A. Grulke, A. Abe, and D. R. Bloch, *Polymer Handbook*, John Wiley & Sons, 2005.
6. F. Walther, P. Davydovskaya, S. Zürcher, M. Kaiser, H. Herberg, A. M. Gigler, and R. W. Stark, *Journal of Micromechanics and Microengineering*, 2007, **17**, 524.
7. S. Park, J. Gobrecht, C. Padeste, H. Schift, K. Vogelsang, U. Pieles, and S. Saxer, .
8. S. Ham, C. Shin, E. Kim, D. Y. Ryu, U. Jeong, T. P. Russell, and C. J. Hawker, *Macromolecules*, 2008, **41**, 6431–6437.
9. NESAC/BIO, .
10. D. J. Graham and D. G. Castner, *Biointerphases*, 2012, **7**.
11. S. Liu, L.-T. Weng, C.-M. Chan, L. Li, N. K. Ho, and M. Jiang, *Surface and Interface Analysis*, 2001, **31**, 745–753.
12. L. T. Weng and C. M. Chan, *Applied surface science*, 2003, **203**, 532–537.
13. L. T. Weng, P. Betrand, W. Lauer, R. Zimmer, and Busetti, S., *Surface and Interface Analysis*, 1995, **23**, 879–886.
14. R. J. Hunter, *Zeta potential in colloid science : principles and applications*, Academic Press, London; New York, 1981.
15. A. Sze, D. Erickson, L. Ren, and D. Li, *Journal of Colloid and Interface Science*, 2003, **261**, 402–410.
16. B. J. Kirby and E. F. Hasselbrink, *Electrophoresis*, 2004, **25**, 187–202.